Vol 16 No 7, July 2007
1009-1963/2007/16(07)/2044-07

Chinese Physics

© 2007 Chin. Phys. Soc.
and IOP Publishing Ltd

RF electric field penetration and power deposition into nonequilibrium planar-type inductively coupled plasmas*

Mao Ming(毛 明), Wang Shuai(王 帅),
Dai Zhong-Ling(戴忠玲), and Wang You-Nian(王友年)

The State Key Laboratory of Materials Modification, Department of Physics, Dalian University of Technology, Dalian 116024, *China*

(Received 13 September 2006; revised manuscript received 23 January 2007)

The RF electric field penetration and the power deposition into planar-type inductively coupled plasmas in low-pressure discharges have been studied by means of a self-consistent model which consists of Maxwell equations combined with the kinetic equation of electrons. The Maxwell equations are solved based on the expansion of the Fourier–Bessel series for determining the RF electric field. Numerical results show the influence of a non-Maxwellian electron energy distribution on the RF electric field penetration and the power deposition for different coil currents. Moreover, the two-dimensional spatial profiles of RF electric field and power density are also shown for different numbers of RF coil turns.

Keywords: inductively coupled plasma, RF field penetration, kinetic theory
PACC: 5250, 5250D, 5250G

1. Introduction

Inductively coupled plasma sources (ICPs) nowadays are widely used in the semiconductor industry for etching and deposition of thin films[1,2] due to the fact that these sources can generate high-density plasmas under low pressures. According to the shape and the position of RF coil, these sources are usually divided into two types, i.e. the planar-type ICP and the cylindrical-type ICP.[3] The planar-type ICP is more popular in the plasma processing for it can easily produce the large-area uniform plasmas . During the past decades, much attention has been paid to the heating mechanism and penetration behaviour of the RF electric field[4−18] for the low-pressure plasmas.

In low-pressure discharges, the collisionless heating is the predominant heating mechanism which was first suggested by Tunrer[4] and later validated in experiment by Godyak and Kolobov.[5] Under this condition, the motion of thermal electron leads to the anomalous penetration of RF field, non-monotonic distribution of the RF electric field, and the negative power absorption,[19] which have been recently proved through the measurements of RF field with a magnetic probe.[20] To investigate the collisionless heating mechanism, Yoon *et al*[8] have deduced a set of one-dimensional analytic formulas in a planar-type ICP discharge, under the assumption of a uniform profile of electron density. This theory was further developed by Kaganovich and Polomarov[17] with a nonuniform electron density model. Although the one-dimensional kinetic simulation can explain most phenomena occurring in the low-pressure ICP discharges, a multi-dimensional simulation is more required to optimize the design of these reactors. In Ref.[21], Yoon *et al* successfully extended their former work to the two-dimensional case by assuming the isotropic electron energy distribution function (EEDF) to be Maxwellian. However, a recent experiment[5] has indicated that the EEDF is non-Maxwellian in the low-pressure discharges, therefore it is necessary to establish a two-dimensional kinetic model to examine the influence of non-Maxwellian distribution on the electric field penetration and the power deposition.

In the present paper, we establish a two-dimensional self-consistent kinetic model to investigate the RF electric field penetration and RF power deposition into the nonequilibrium uniform planar-type inductively coupled discharges. The detailed description of the kinetic two-dimensional model is pre-

*Project supported by the National Natural Science Foundation of China (Grant Nos 10376003 and 10572035).

sented in Section 2. The numerical results as well as discussion are given in Section 3, while the main conclusions are summarized in Section 4.

2. Theory

The schematic diagram of a typical planar-type ICP reactor along with the adopted coordinate is shown in Fig.1.

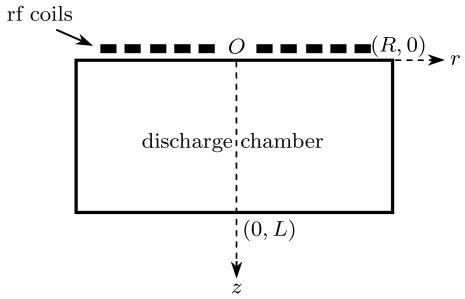


Fig.1. The schematic diagram of a planar-type ICP reactor along with the adopted coordinate.

The discharge chamber is a cylinder with the radius R and the height L. A multi-turn RF coil is placed on the top of the chamber, driven by an RF source, and it generates a transverse RF field $\boldsymbol{E}$ maintaining the plasma discharge. According to the cylindrical symmetry of the reactor, the RF field $\boldsymbol{E}$ only has the azimuthal component, i.e.

$$\boldsymbol{E}(\boldsymbol{r},t) = E_\phi(r,z)\exp(-\mathrm{i}\omega t)\boldsymbol{e}_\phi, \tag{1}$$

where RF field is assumed to vary with time in the form of $\mathrm{e}^{-\mathrm{i}\omega t}$.

The boundary conditions for the RF electric field are

$$\begin{cases} E_\phi(R,z,t)=0, \\ E_\phi(r,L,t)=0, \\ E_\phi(0,z,t)=0, \end{cases} \tag{2}$$

$E_\phi(r,z)$ could be expanded with the Fourier–Bessel series as [21]

$$E_\phi(r,z) = \sum_{m=1}^{\infty}\left[J_1(P_m r/R)\sum_{s=0}^{\infty} e_{ms}\cos(k_s z)\right], \tag{3}$$

where e_{ms} is the expanding coefficient, $J_1(x)$ is the Bessel function of the first kind of order one, P_m is the mth root of $J_1(x)=0$, and the wave number k_s is expressed as

$$k_s = \left(s+\frac{1}{2}\right)\pi/L, \quad s=0,1,2,3\cdots. \tag{4}$$

We also assume that the electrons specularly reflect from the bottom boundary $z=L$ and neglect the ambipolar electric field in the following deduction.

The electron Boltzmann equation reads

$$\frac{\partial f(\boldsymbol{r},\boldsymbol{v},t)}{\partial t} + \boldsymbol{v}\cdot\nabla_{\boldsymbol{r}} f(\boldsymbol{r},\boldsymbol{v},t) - \frac{e}{m_\mathrm{e}}(\boldsymbol{E}+\boldsymbol{v}\times\boldsymbol{B})\cdot\frac{\partial f(\boldsymbol{r},\boldsymbol{v},t)}{\partial \boldsymbol{v}} = S(f), \tag{5}$$

where $S(f)$ is the collision integral, $\boldsymbol{v}$, e and m_e are electron velocity, unit charge, and electron mass, respectively. Using the two-term approximation,[17] the electron energy distribution function $f(\boldsymbol{r},\boldsymbol{v},t)$ is represented by sum of two terms and expressed as $f(\boldsymbol{r},\boldsymbol{v},t) = f_0(\varepsilon) + f_1(\boldsymbol{r},\boldsymbol{v},t)$. Here $f_0(\varepsilon)$ is the isotropic distribution function, $\varepsilon = \frac{1}{2}m_\mathrm{e}v^2$ is the total energy of electron, and $f_1(\boldsymbol{r},\boldsymbol{v},t)$ is the perturbed distribution function. Notice $\boldsymbol{v}\times\boldsymbol{B}\cdot\frac{\partial f(\boldsymbol{r},\boldsymbol{v},t)}{\partial \boldsymbol{v}} = 0$, thus Eq.(5) becomes

$$\frac{\partial f_1}{\partial t} + \boldsymbol{v}\cdot\nabla_{\boldsymbol{r}} f_1 - \frac{e}{m_\mathrm{e}}\boldsymbol{E}\cdot\frac{\partial f_0}{\partial \boldsymbol{v}} = S_1(f_1), \tag{6}$$

$$-\frac{e}{m_\mathrm{e}}\left\langle \boldsymbol{E}\cdot\frac{\partial f_1^*}{\partial \boldsymbol{v}}\right\rangle = \langle S_0(f_0)\rangle, \tag{7}$$

where $\langle ...\rangle$ describes averaging over all the phase space available for the electron with the total energy ε.[17] In the planar-type ICP discharge, the electric field generated by the top coil transmits into the plasma mainly along the z- direction, hence the change of the perturbed distribution function f_1 along the r- direction is much smaller than that in the z- direction, i. e. $\left|\frac{\partial f_1}{\partial r}\right| \ll \left|\frac{\partial f_1}{\partial z}\right|$. Therefore, Eq.(6) turns to

$$\frac{\partial f_1}{\partial t} + v_z\frac{\partial f_1}{\partial z} - \frac{e}{m_\mathrm{e}}E_\phi\frac{\partial f_0}{\partial v_y} = -\nu_m f_1, \tag{8}$$

where the Bhatnager–Gross–Krook (BGK) approximation $S_1(f_1) = -\nu_m f_1$ has been used, and ν_m is the momentum transfer collision frequency. Following the method in Ref.[16], we transform the perturbed velocity function f_1 with the Fourier series as follows:

$$f_1(r,z,\boldsymbol{v},t) = \sum_{n=-\infty}^{\infty} F_n(r,z,\boldsymbol{v})\exp\left[\mathrm{i}n\alpha(z)\right], \tag{9}$$

where $\alpha(z)$ is taken as

$$\alpha(z) = \mathrm{sgn}(v_z)\frac{\pi}{L}z, \tag{10}$$

which is called 'reflection angle',[17] and

$$\mathrm{sgn}(v_z)=\begin{cases}1 & v_z>0,\\ -1 & v_z<0.\end{cases} \tag{11}$$

Substituting expressions (9)–(11) into Eq.(8), we obtain the expression for f_1 as follows:

$$f_1(r,z,\boldsymbol{v},t)=\frac{e}{m_\mathrm{e}}\sum_{n=-\infty}^{\infty}\left[\frac{E_n\mathrm{e}^{\mathrm{i}n\alpha(z)-\mathrm{i}\omega t}}{\nu_m-\mathrm{i}\omega+\mathrm{i}n\Omega}\right]\frac{\partial f_0}{\partial v_y}, \tag{12}$$

where the reflection frequency $\Omega=\pi\left|v_z\right|/L$ and the Fourier coefficient E_n are given as

$$E_n=\frac{1}{2\pi}\sum_{m=1}^{\infty}J_1\left(P_m\frac{r}{R}\right)\sum_{s=0}^{\infty}e_{ms}G_{sn}, \tag{13}$$

$$G_{sn}=\frac{(-1)^{s-n}(2s+1)}{\left(s+\dfrac{1}{2}\right)^2-n^2}. \tag{14}$$

Once the expression for perturbed distribution function $f_1(r,z,\boldsymbol{v},t)$ is known, we can easily obtain the equation for $f_0(\varepsilon)$. Substituting expression (13) into Eq.(7), and then averaging over the period of electron bouncing and all possible perpendicular velocities,[22] we have

$$-\frac{\mathrm{d}}{\mathrm{d}\varepsilon}\left[\left(D_E+\bar{D}_{\mathrm{ee}}\right)\frac{\mathrm{d}f_0}{\mathrm{d}\varepsilon}\right]-\frac{\mathrm{d}}{\mathrm{d}\varepsilon}\left[\left(\bar{V}_{\mathrm{el}}+\bar{V}_{\mathrm{ee}}\right)f_0\right]=\sum_q\left[\sqrt{\varepsilon+\varepsilon_q^*}\nu_q^*\left(\varepsilon+\varepsilon_q^*\right)f_0\left(\varepsilon+\varepsilon_q^*\right)-\sqrt{\varepsilon}\nu_q^*\left(\varepsilon\right)f_0\left(\varepsilon\right)\right], \tag{15}$$

where $D_E(\varepsilon)$ is the energy transfer coefficient, which is expressed as

$$D_E(\varepsilon)=\frac{e^2\varepsilon^{3/2}}{2m_\mathrm{e}}\sum_{n=-\infty}^{\infty}\sum_{m=1}^{\infty}\left|e_{mn}\right|^2\left[J_1'(P_m)\right]^2\Psi\left(\alpha,\beta\right), \tag{16}$$

$$e_{mn}=\sum_{s=0}^{\infty}e_{ms}G_{ns}. \tag{17}$$

Here $J_1'(x)$ is the derivative of $J_1(x)$, $\alpha=n\Omega_0/\omega$, $\beta=\nu_m/\omega$, $\Omega_0=\pi v/L$, ε_q^* is the threshold energy for the qth energy state, $\nu_q^*(\varepsilon)$ is the inelastic collision frequency, and the expressions for $\bar{D}_{\mathrm{ee}}$, $\bar{V}_{\mathrm{el}}$, $\bar{V}_{\mathrm{ee}}$ could be found in Ref.[22]. $\Psi(\alpha,\beta)$ is the function describing the interaction between the RF electric field and plasma electrons, and satisfies

$$\Psi\left(\alpha,\beta\right)=\frac{\left(\alpha^2+\beta^2-1\right)}{\alpha^3}\left[\mathrm{arctg}\left(\frac{1+\alpha}{\beta}\right)-\mathrm{arctg}\left(\frac{1-\alpha}{\beta}\right)\right]. \tag{18}$$

In order to determine the coefficient $D_E(\varepsilon)$, we must solve the expanding coefficient e_{ms} first. Utilizing the Maxwell equations

$$\begin{cases}\bigtriangledown\times\boldsymbol{E}=-\dfrac{\partial\boldsymbol{B}}{\partial t},\\ \bigtriangledown\times\boldsymbol{B}=\mu_0\left(\boldsymbol{j}+\boldsymbol{I}_\mathrm{c}\right)+\varepsilon_0\mu_0\dfrac{\partial\boldsymbol{E}}{\partial t},\end{cases} \tag{19}$$

where $\boldsymbol{j}$ is the electron current in plasma and $\boldsymbol{I}_\mathrm{c}$ is the current in the coils. Further, we obtain the wave equation

$$\left[\frac{\partial^2}{\partial r^2}+\frac{1}{r}\frac{\partial}{\partial r}-\frac{1}{r^2}+\frac{\partial^2}{\partial z^2}+\frac{\omega^2}{c^2}\right]E_\phi(r,z)$$

$$=-\frac{\mathrm{i}\omega}{\varepsilon_0c^2}[j_\phi(r,z)+I_\mathrm{c}(r)\delta(z)], \tag{20}$$

where

$$j_\phi(r,z)=-en_0\int\mathrm{d}\boldsymbol{v}f_1(r,z,\boldsymbol{v}), \tag{21}$$

$\delta(z)$ is the Dirac delta function, $I_\mathrm{c}(r)$ is determined by the specific parameter of the coil, and taken as $I_\mathrm{c}(r)=I\sum_{c=1}^{N_\mathrm{c}}\delta\left(r-r_c\right)$ for simplification. I is the amplitude of coil current, r_c is the position of the cth coil, and N_c is the turn number of RF coil. Inserting expressions (3), (12) and (21) into Eq.(20), we obtain the equation of e_{ms} as follows:

$$\left(\frac{\omega^2}{c^2}-k_s^2-\frac{P_m^2}{R^2}\right)e_{ms}=-\mathrm{i}\omega\mu_0\left[\sum_{s'=0}^{\infty}e_{ms'}W_{ss'}+\sum_{c=1}^{N_\mathrm{c}}\frac{4Ir_cJ_1\left(r_c/R\right)}{LR^2J_2^2\left(P_m\right)}\right], \tag{22}$$

where

$$W_{ss'}=-\frac{\varepsilon_0\omega_\mathrm{p}^2}{\omega}\sum_{n=0}^{\infty}G_{sn}G_{s'n}\int_0^{\infty}\mathrm{d}\varepsilon\varepsilon^{\frac{3}{2}}\left[\Psi\left(\alpha,\beta\right)+\mathrm{i}\Phi\left(\alpha,\beta\right)\right]\frac{\mathrm{d}f_0}{\mathrm{d}\varepsilon}, \tag{23}$$

and

$$\begin{aligned}\Phi(\alpha,\beta)=\ &\frac{(\alpha^2+\beta^2-1)}{2\alpha^3}\ln\left[\frac{(\alpha-1)^2+\beta^2}{(\alpha+1)^2+\beta^2}\right]-\frac{2}{\alpha^2}\\&+\frac{1}{\alpha^3}\left\{-2\beta\left[\mathrm{arctg}\left(\frac{1+\alpha}{\beta}\right)-\mathrm{arctg}\left(\frac{1-\alpha}{\beta}\right)\right]\right\}.\end{aligned} \tag{24}$$

Once the RF electric field $E_\phi\left(r,z,t\right)$ and the RF current $j_\phi(r,z,t)$ are determined, the absorbed power density $P(r,z)$ may be calculated by

$$P(r,z)=\frac{1}{2}\left[\mathrm{Re}j_\phi^*(r,z,t)\cdot E_\phi(r,z,t)\right]. \tag{25}$$

Now, we have achieved a system of equations to determine the electron energy distribution function (EEDF) f_0, the profiles of the RF electric field E_ϕ, and the power density P self-consistently.

3. Results and discussion

In this section, we present the numerical results of the electron energy distribution function, the RF electric field profiles, and the power deposition in the planar-type ICP argon discharge. From the deduction in Section 2, we notice that there are seven parameters that should be input before the calculation, such as the plasma density n_0, height of the reactor L, radius R, gas pressure p, driving frequency of coil ω, coil current I, and turn number of the coil N_c. In this paper, we only consider the influences of the current I and the turn number N_c, and the other parameters chosen in the calculation are $n_0=1.5\times10^{11}\,\mathrm{cm}^{-3}$, $L=10.5\,\mathrm{cm}$, $R=9.9\,\mathrm{cm}$, $p=0.13\,\mathrm{Pa}$, and $\omega=2\pi\times13.56\,\mathrm{MHz}$. When we calculate the profiles of the RF field and power density using the Maxwellian distribution, the electron temperature T_e is set as 3.2 eV.

The evolution of EEDF as a function of energy ε for different values of I is shown in Fig.2, and the Maxwellian distribution is also plotted for comparison. Here the turn number is taken as $N_\mathrm{c}=5$, the positions of each coil are $r_1=2.2\,\mathrm{cm}$, $r_2=3.2\,\mathrm{cm}$, $r_3=4.1\,\mathrm{cm}$, $r_4=5.1\,\mathrm{cm}$, $r_5=6\,\mathrm{cm}$, respectively. Under the low pressure of 0.13 Pa, the EEDF presents a three-temperature structure with low temperature for an energy of a few eV, high temperature for a moderate energy between 5 eV and 20 eV, and for higher temperature for an energy beyond 20 eV, which is different from that for the Maxwellian distribution. As current I increases, more energies are transferred into the plasma and the EEDF becomes a bi-Maxwellian.

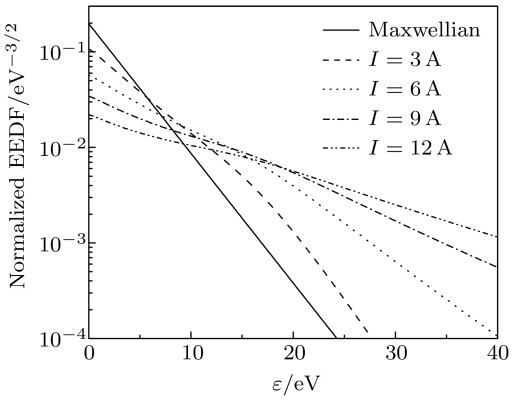


Fig.2. The evolution of the normalized EEDF as a function of energy ε for different values of coil current I.

The profiles of the RF electric field at $r=5.3\,\mathrm{cm}$ as a function of height z for different values of current I are shown in Fig.3 for the cases of (a) self-consistent model and (b) Maxwellian distribution, where $\omega t=0$. Different from the monotonous attenuation calculated from the Maxwellian distribution, the RF electric field displays a non-monotonous decline. The electric field decays rapidly near the coil (about 2 cm apart), and

then reaches its first minimum followed by a local maximum. This anomalous electric field penetration has been reported by several authors.[5,9,22] As the amplitude of coil current I increases, the anomalous penetration of the RF electric field becomes more notable. At a pressure of 0.13 Pa, the electron collision mean free path is much larger than the dimension of reactor, therefore electrons move in a collisionless manner. After obtaining the energy from the RF electric field, the energetic electrons move into the bulk plasma under the action of force $\boldsymbol{E} \times \boldsymbol{B}$ without collision. When the velocity of the electrons is comparable with the phase velocity of electromagnetic wave, the Landau dumping occurs, resulting in the anomalous penetration of the RF electric field.

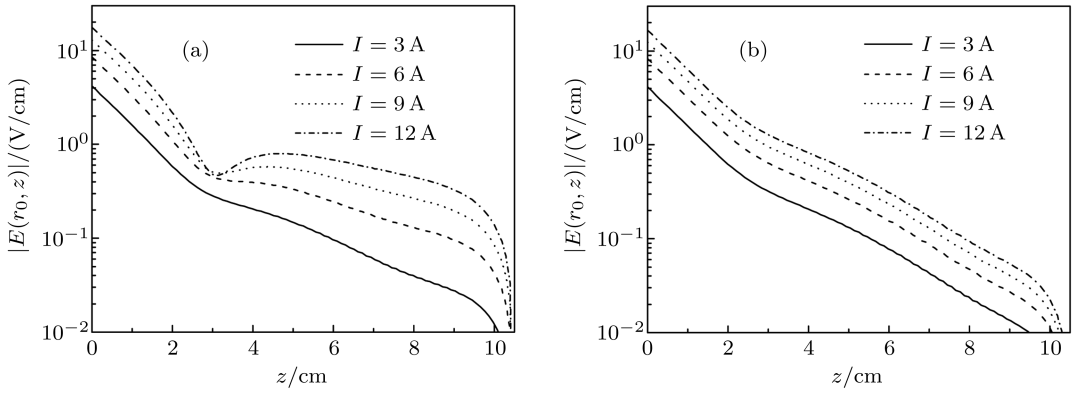


Fig.3. Comparison between the RF electric field profiles calculated from (a) self-consistent model and (b) Maxwellian distribution for different values of I at $r = 5.3$ cm.

The power depositions as a function of height z for different values of coil current I at $r = 5.3$ cm are shown in Fig.4 for the cases of (a) self-consistent model and (b) Maxwellian distribution. The negative power absorption can be observed from the results calculated both from the self-consistent model and from the Maxwellian distribution. In the collisionless regime, due to the strong interaction between RF field and plasma electrons, the phase difference between the RF field and plasma current exceeds 90° and leads to a negative power absorption. Unlike the results from the Maxwellian distribution, the region of the negative power absorption moves away from the coil as the value of I increases. Moreover, the skin layer for the power deposition is also expanding toward the bulk plasma as coil current I is enhanced. Comparing our results with the measure in Ref.[19], a qualitative agreement between them can be obtained.

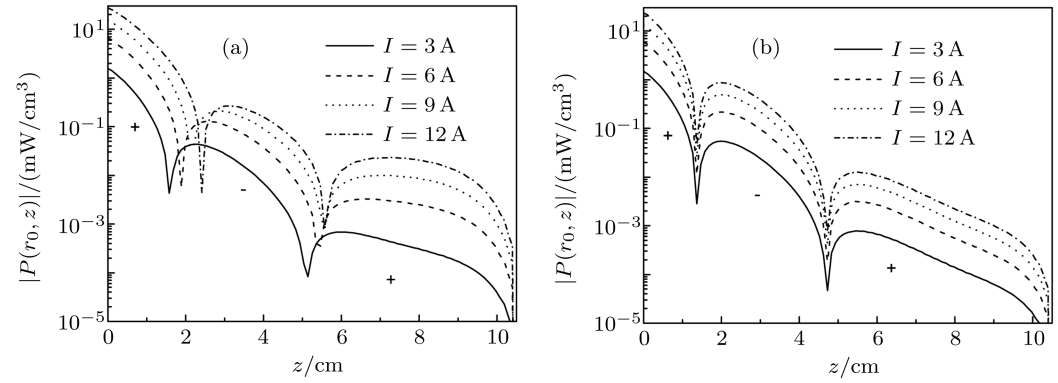


Fig.4. Comparison between the RF power depositions calculated from (a) self-consistent model and (b) Maxwellian distribution for different values of I at $r = 5.3$ cm.

Figures 5(a) and 5(b) show a two-dimensional spatial profile of RF electric field at $I = 5$ A and $\omega t = 0$ for different turn numbers of coil where the self-consistent model is adopted. In the simulation, we regards the RF coils as a set of homocentric rings with azimuthal symmetry, this is an assumption usually adopted in simulation.[21] The electric fields display local maxima at the position of each coil in the

$r-$ direction, due to the boundary conditions where the electric fields at both the centre and the chamber wall are zero. Because of the superposition of electric fields generated by each coil, the electric field at the position of the middle coil has a larger amplitude than on the side of coil. The profile of the electric field, featured by such as the width of the peak and the gap between local maxima, is mainly determined by the specific coil parameters. We also find that as the turn number of coil increases, the strength and uniformity of the RF electric field in the r- direction are enhanced. A similar trend is also found in the distributions of power deposition (see Figs.6(a) and 6(b)). Therefore, in order to obtain a large-area uniform plasma, optimizing the design of the RF coils is very important.

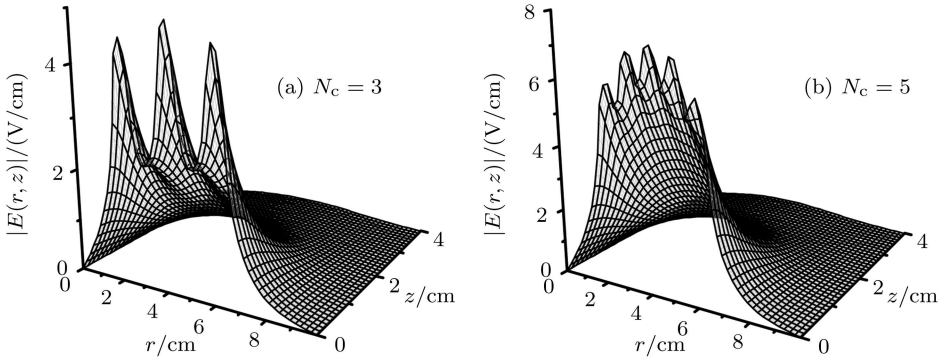


Fig.5. The spacial distribution of the RF electric fields for (a) $N_c = 3$ and (b) $N_c = 5$ at $I = 5$ A.

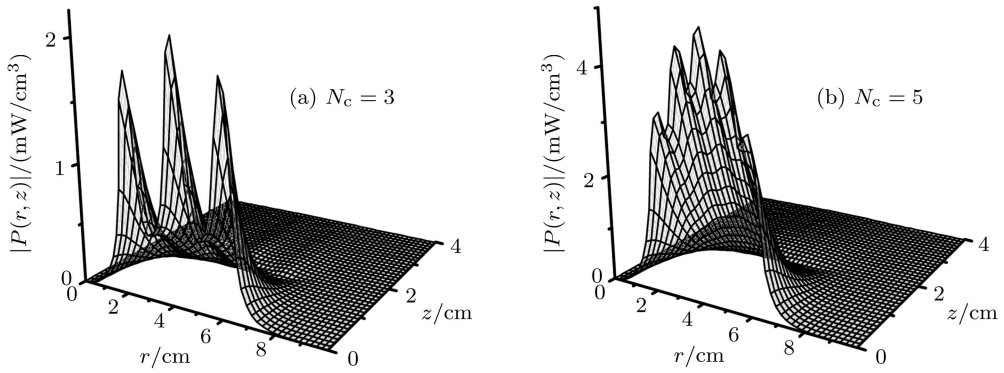


Fig.6. The spacial profile of the RF power densities for (a) $N_c = 3$ and (b) $N_c = 5$ at $I = 5$ A.

4. Summary

In order to investigate the RF electric field penetration and power deposition into nonequilibrium planar-type inductively coupled plasmas, a self-consistent model which consists of electron Boltzmann equation and Maxwell equation has been developed. The numerical results indicate that the electron energy distribution function (EEDF) is no longer Maxwellian in the low pressure ICP discharges, therefore the linear model (where the EEDF is assumed to be Maxwellian) in these discharges will be not valid. The influences of specific coil parameters on the electric field penetration and power deposition are also discussed in this paper, and some experimental phenomena such as negative power absorption are shown with our model. While the RF antenna used in the ICP source is planar spiral, which leads to a nonuniform plasma in the azimuthal direction, so a 3D model is needed.

All the results presented here are expected to be helpful to understanding the phenomena observed in recent experiment of inductively coupled plasma, and also to optimizing the design of planar-type ICP reactor.

References

[1] Liberman M A and Lichtenberg A J 1994 *Principles of Plasma and Materials Processing* (New York: Wiley) p388

[2] Xin Y, Di X L, Yu Y Q and Ning Z Y 2006 *Acta Phys. Sin.* **55** 3494 (in Chinese)

[3] Graves D B 1994 *IEEE Trans. Plasma Sci.* **22** 1
Graves D B 1994 *IEEE Trans. Plasma Sci.* **22** 31

[4] Turner M M 1993 *Phys. Rev. Lett.* **71** 1844

[5] Godyak V A and Kolobov V I 1998 *Phys. Rev. Lett.* **81** 369

[6] Kortshagen U, Pukropski I and Zethoff M 1994 *J. Appl. Phys.* **76** 2048

[7] Kolobov V I and Hitchon W N G 1995 *Phys. Rev.* E **52** 972

[8] Yoon N S, Kim S S, Chang C S and Choi D I 1996 *Phys. Rev.* E **54** 757

[9] Kolobov V I, Lymberopoulos D P and Economou D J 1997 *Phys. Rev.* E **55** 3408

[10] Chung C W, Kim S S, Seo S H, Chang H Y and Yoon N S 2000 *J. Appl. Phys.* **88** 1181

[11] Godyak V A, Piejak R B, Alexandrovich B M and Kolobov V I 1998 *Phys. Rev. Lett.* **80** 3264

[12] Godyak V A, Piejak R B and Alexandrovich B M 1999 *J. Appl. Phys.* **85** 703

[13] Godyak V A, Piejak R B and Alexandrovich B M 1999 *Phys. Rev. Lett.* **83** 1610

[14] Seo S H, Chung C W, Hong J I and Chang H Y 2000 *Phys. Rev.* E **62** 7155

[15] Chung C W and Chang H Y 2000 *Phys. Plasma* **7** 3826

[16] Godyak V A, Piejak R B and Alexandrovich B M 2002 *Plasma Sources Sci. Technol.* **11** 525

[17] Kaganovich I D and Polomarov O 2003 *Phys. Rev.* E **68** 026411

[18] Ramamurthi B, Economou D J and Kaganovich I D 2003 *Plasma Sources Sci. Technol.* **12** 302

[19] Godyak V A and Kolobov V I 1997 *Phys. Rev. Lett.* **79** 4589

[20] Godyak V A and Piejak R B 1997 *J. Appl. Phys.* **82** 1

[21] Yoon N S, Hwang S M and Choi D I 1997 *Phys. Rev.* E **55** 7536

[22] Mao M and Wang Y N 2005 *Plasma Sci. & Technol.* **7** 2640